Hindawi
International Journal of Energy Research
Volume 2023, Article ID 8659009, 13 pages
https://doi.org/10.1155/2023/8659009

Research Article

Electrical Double-Layer Capacitor Based on Low Aqueous Electrolyte Contents in EmimTFO Ionic Liquid

V. N. Kitenge,[1] D. J. Tarimo,[2] K. O. Oyedotun,[2] G. Rutavi,[2] D. T. Bakhoum,[2] and N. Manyala[2]

[1]*Department of Chemical Engineering, University of Pretoria, Pretoria 0028, South Africa*
[2]*Department of Physics, Institute of Applied Materials, SARChI Chair in Carbon Technology and Materials, University of Pretoria, Pretoria 0002, South Africa*

Correspondence should be addressed to N. Manyala; ncholu.manyala@up.ac.za

Received 15 February 2023; Revised 11 April 2023; Accepted 13 April 2023; Published 25 April 2023

Academic Editor: Pranav Kalidas Katkar

A study has been conducted on the electrochemical properties of 1-ethyl-3-methylimidazolium trifluoromethanesulfonate (EmimTFO) protic ionic liquid enhanced by adding potassium nitrate (2.5 M) aqueous solution. The properties of EmimTFO as well as mixtures diluted by molar fractions of 0.6, 0.7, 0.8, and 0.9 of KNO_3 were also investigated through measurements of viscosity, density, and conductivity. In a three-electrode test run at 0.25 A g^{-1}, the addition of 2.5 M KNO_3 solution generated peak specific capacities of ~40.2 and ~85.8 mAh g^{-1} on the positive and negative potentials, respectively. These performances surpassed the specific capacities obtained for EmimTFO in a three-electrode run at 0.25 A g^{-1} using the same electrode material (activated carbon). The top-performing electrolyte mixture ($[EmimTFO]_{0.8}[2.5\,M\ KNO3]_{0.2}$) was then used to assemble a symmetric supercapacitor, which could run at a voltage of ~2.1 V. The device was able to retain 71.35% of its capacitance after 10,000 cycles of charge and discharge. It also displayed higher specific energy and power of 22.21 Wh kg^{-1} and 520 W kg^{-1}, respectively, at 0.5 A g^{-1} as compared to specific energies of 4.73 Wh kg^{-1} and 11.2 Wh kg^{-1} for the devices assembled with single EmimTFO and 2.5 M KNO_3 as the electrolytes, respectively.

1. Introduction

Seeking effective, dependable, and economical electrochemical energy devices is still a global essential responsibility [1, 2]. Promising energy storage technologies, involving both physical and chemical energies, are being studied to alleviate the challenge of a continuous energy supply. Supercapacitors (SCs) make part of the leading technologies for energy storage [3]. SCs are known for their superior specific power output, reasonable production cost, safety, and long cycle life [4]. Electrodes and electrolytes are the key components of SCs that could impact their performances [5, 6]. Developing novel electrode materials or electrolytes can result in improving SCs' specific energy [7].

Electric double-layer capacitors (EDLCs) are typical supercapacitors. EDLC electrode materials exhibit excellent electrical conductivity and have a high specific surface area which allows them to efficiently store charge [8]. These properties promote EDLCs' charge storage mechanism which is accomplished through swift electrostatic adsorption of electrolyte ions on the surface of the electrode, resulting in the formation of an electric double layer (EDL) at the juncture between the electrode and electrolyte [9]. One such material that is commonly used in EDLCs is activated carbon (AC). EDLCs have a notable drawback which is their lower energy density compared to other types of capacitors. The energy density of EDLCs is closely tied to the operating voltage range of the device. Therefore, it is essential to design electrolytes that allow wide potential windows while also offering high ionic conductivity to achieve optimal performance [10]. Ionic liquids (ILs) are a cutting-edge category of electrolytes used in energy storage devices, particularly in supercapacitors. [11]. These electrolytes enable higher cell potential (U) which in turn enhances the specific energy (E)

in energy storage devices as per the formula: $E = 1/2C \cdot U^2$ (C – capacitance). The chemical structure of ILs categorizes them as aprotic (AILs) or protic (PILs) ionic liquids. PILs differ from AILs because they can carry one or more protons on their cation or anion, whereas AILs cannot [12]. ILs demonstrated great electrochemical stability when used as electrolytes in SCs [13–15]. They possess a wider potential window than traditional aqueous and organic electrolytes. However, their room-temperature ionic conductivity is typically lower than that of these other electrolytes [16]. This is due to their viscous nature which restricts their use in their pure form at room temperature [17]. Preparing mixtures of previously recognized ILs for energy storage applications is one technique for improving their transport properties [18–20]. Mixtures of ILs with other types of solvents have also been explored. A study by Palm et al. [21] revealed that incorporating 16% by weight of acetonitrile (AN) into 1-ethyl-3-methylimidazolium tetrafluoroborate ($EmimBF_4$) decreased the $EmimBF_4$'s viscosity by 20% while also significantly increasing the mixture's conductivity by 2.5 times. Chaban [22] also found that adding AN to several imidazolium ILs improves their conductivity by up to 50 times their original values. Sethuraman and Montree [23] reported a dual ionic liquid (IL) and 1.0 M LiTFSI (aq.) "water in salt" mixture with enhanced specific capacitance and specific energy as compared to ionic liquid electrolyte alone.

Not much studies in the literature have explored the addition of water-based (aqueous) electrolytes (potassium nitrate, potassium hydroxide, sodium hydroxide, and so on) to improve IL properties. This present work analyzes, for the first time, the electrochemical properties of an innovative electrolyte mixture made up of 1-ethyl-3-methylimidazolium trifluoromethanesulfonate (EmimTFO) and 2.5 M KNO_3, at different molar ratios of 0.6, 0.7, 0.8, and 0.9. EmimTFO (PILs) was selected due to its hydrophilic and protic nature, which is advantageous for dilution with the aqueous electrolyte. To investigate the electrochemical properties of these mixtures, techniques such as impedance spectroscopy (EIS), galvanostatic charge-discharge (GCD), and cyclic voltammetry (CV) were used to evaluate the performance of the IL/aqueous mixtures as electrolytes in a three- and two-electrode configuration, where AC was utilized as the electrode material. As PILs mainly carry available protons, these electrolytes allow mixtures to combine them with an aqueous medium through hydrogen bonding to form the Grotthuss like protons [24]. The mixture may also prevent the use of highly flammable, volatile organic solvents while obtaining an economical electrolyte with high potential windows. The electrolyte mixture has illustrated an interesting electrochemical feature that unlocks the limits of aqueous electrolyte and ionic electrolyte systems, providing an important direction for the development of high-energy supercapacitors.

2. Experimental

EmimTFO IL ($H_2O < 20$ ppm, 99.9%) was obtained from Solvionic (Toulouse, France). Deionized (DI) water was utilized to prepare the 2.5 M KNO_3 solution. KNO_3 was purchased from Sigma Aldrich (Missouri, United States). The four $[EmimTFO]_x[2.5\ M\ KNO_3]_{(1-x)}$ electrolyte mixtures were prepared via magnetic stirring at 120 rpm for 1 hour (h) within a glovebox (provided by Inert Technologies, USA) which ensured that the oxygen and water levels were maintained at 0.0%. The x in the $[EmimTFO]_x[2.5\ M\ KNO_3]_{(1-x)}$ formula represents the ionic liquid's molar fraction, and 1-x the 2.5 M KNO_3 molar fraction in the solutions. The prepared mixtures are: (1) $[EmimTFO]_{0.9}[2.5\ M\ KNO_3]_{0.1}$, (2) $[EmimTFO]_{0.8}[2.5\ M\ KNO_3]_{0.2}$, (3) $[EmimTFO]_{0.7}[2.5\ M\ KNO_3]_{0.3}$, and (4) $[EmimTFO]_{0.6}[2.5\ M\ KNO_3]_{0.4}$, respectively.

The conductivities of EmimTFO, 2.5 M KNO_3, and the mixtures were determined using a Jenco model 3020M conductivity meter (Jenco, USA) with conductivity accuracy of ~0.5 F. S at a temperature of 18.2°C. The viscosities were evaluated using an RV model NDJ-8S viscometer (W & J Instrument Co., PRC). The densities (ρ) were measured using an Attension model Sigma 700 densimeter (KSV Instrument, Finland).

Activated carbon derived from mangosteen shell (MS-AC), which was synthesized in our previous work, was used as the electrode material. A one-step carbonization/activation method was used to synthesize the material from the mangosteen shells (MS) [25]. The synthesis process involved pyrolyzing a mixture of 5 grams (g) of mangosteen shells and 5 g of K_2CO_3 (activating agent) in a tubular furnace. The furnace was set to a temperature of 700°C and heated at a ramp rate of 5°C per minute for 2 h while argon gas was flown at 200 $cm^3\ min^{-1}$. Postsynthesis, the material was filtered, thoroughly rinsed until a neutral pH was attained, and dried at 60°C for a period of 12 h. Figure 1 displays the textural properties obtained with MS-AC. These properties were analyzed using a NOVA touch LX^2 Quanta chrome pore size distribution and surface area analyzer (NOVA touch NT 2 LX-1, 220 V, USA). The Brunauer-Emmett-Teller (BET) method was used to evaluate the material's specific surface area through isotherms of adsorption and desorption, utilizing a relative pressure (P/Po) range of 0.05 to 0.95 (as depicted in Figure 1(a)). The density functional theory (DFT) method enabled determining the material's pore-size distribution (as seen in Figure 1(b)). The results illustrated the type-I isotherm with an H4 hysteresis loop, representing a high percentage of micropores and mesopores in the MS-AC. The morphological image of the sample, as seen in the inset, was acquired with a Zeiss Ultra Plus 55 field emission scanning electron microscope (FE-SEM, Akishimashi, Japan) set at 2.0 kV. The image displays a flower-like morphology having a mesoporous arrangement with open cavities. Table 1 indicates the different textural features obtained from the material.

In order to prepare the electrodes, a blend of 80% active material, 10% polyvinylidene difluoride (PVDF) as a binder, and 10% conductive carbon acetylene black (CAB) was made. A total of 3.2 mg of electrode material was used per electrode, consisting of 2.56 mg of active material (activated carbon), 0.32 mg of CAB, and 0.32 mg of PVDF. CAB was added to boost the conductivity lost due to the presence of the nonconductive PVDF. The mixture was then made homogenous by producing a slurry with the addition of two 0.5 ml drops of N-methyl-2-pyrrolidone (NMP). This

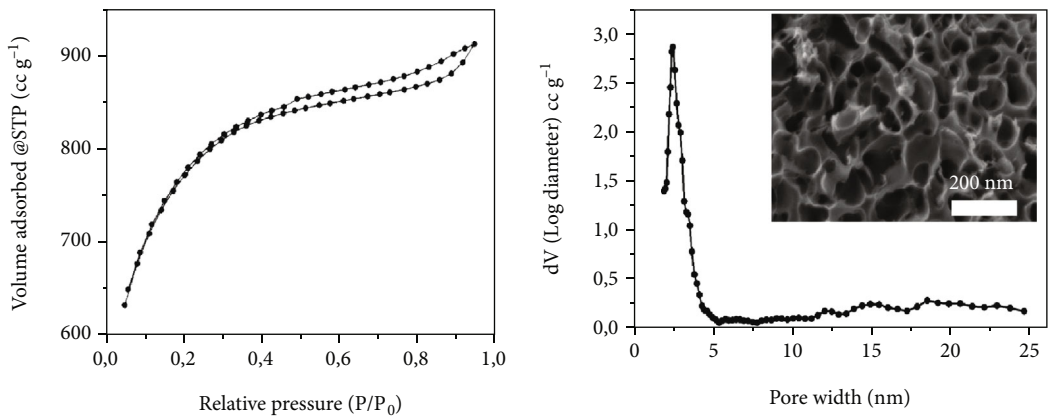

Figure 1: Porous structure of the MS-AC: (a) isotherms illustrating adsorption and desorption using N_2 and (b) pore size distribution determined with DFT (inset showing scanning electron microscopy image) for MS-AC.

Table 1: MS-AC N_2 sorption results using liquid nitrogen.

Surface area	Micropore volume	Total pore volume	Average pore size
2802.57 $m^2 g^{-1}$	0.98 cc g^{-1}	1.41 cc g^{-1}	2.1 nm

slurry was then coated on the surface of a 1 cm^2 nickel foam current collector. The produced electrodes were finally dried in an electric furnace for 12 h at 60°C.

The measurements were conducted at room temperature using a Biologic VMP300 potentiostat (made in the USA) ran with EC-Lab® V11.33 software. The measurements were completed in both a three-electrode and a two-electrode configuration. The three-electrode comprised a T-cell consisting of the fabricated electrode as the working electrode, a silver (Ag) disc used as the reference electrode, and a glassy carbon disc used as the counter electrode. Except from the aqueous-assembled T-cell, all the T-cells made for three-electrode measurements were assembled in the glovebox with all three components separated by filter paper. Before assembly, the electrodes were vacuum-dried at 60°C for 10 hours. The mass of the active material used in the electrodes varied between 2.5 and 2.8 mg cm^{-2} for all the materials under study. CV measurement was carried out at various scan rates within a potential window ranging from -1.6 to 0.0 V for the negative electrode and 0.0 to 1 V for the positive electrode, with both potentials relative to the reference electrode. The GCD test was performed at different specific currents for both the positive and negative tests. EIS was evaluated at frequencies ranging from 10 mHz to 100 kHz at open-circuit potentials.

2.1. Calculations. The specific capacitances (C_{sp}) in the three electrodes for EDLC material were obtained from GCD curves using the following equation:

$$C_{sp} = \frac{I\,\Delta t}{\Delta V\, m}\left(F g^{-1}\right), \tag{1}$$

where m is the mass of the electrodes (mg); I is the applied current (mA), Δt is the discharge time (s); and ΔV is the potential window (volt: V).

For nonlinear GCD curves, the specific capacities (Q_s) calculated in the three electrodes were determined as per the following formula:

$$Q_s = \frac{I\Delta t}{3.6m}\left(mAh\, g^{-1}\right), \tag{2}$$

where Q_s specific is the discharge capacity (mAh g^{-1}); Δt is the discharge time (s); I is the applied current (mA); and m is the active material mass (g).

Equation (3) was used to estimate how much charge is stored on each electrode as follows:

$$\frac{m_+}{m_-} = \frac{Q_{s-}}{Q_{s+}}. \tag{3}$$

The specific capacitance of single electrode (C_{single}) for different symmetric devices GCD curves which showed EDLC behaviour was obtained using the following equation:

$$C_{\text{single}} = \frac{4\,I\,\Delta t}{\Delta V\, M}, \tag{4}$$

where M is the overall mass of both electrodes; I is the applied current, Δt is the discharge time, and ΔV is the voltage of the device.

The specific energy (E_s) and specific power (P_s) of symmetric devices were obtained using the following equations:

$$E_s = \frac{1}{2}C_{\text{single}}(\Delta V)^2 = \frac{1000 \times C_{\text{single}} \times (\Delta V)^2}{2 \times 4 \times 3600} = \frac{C_{\text{single}}\Delta V^2}{28.8}\left(\text{Wh kg}^{-1}\right),$$

$$P_s = 3600 \times \frac{E_d}{\Delta t}\left(\text{W kg}^{-1}\right), \tag{5}$$

where C_{sp} is the device capacitance, ΔV is the device voltage, and Δt is the device's discharge time.

The Coulombic efficiencies were calculated through the following method:

$$\epsilon = \frac{\Delta t \text{ discharge}}{\Delta t \text{ charge}} \times 100\%. \quad (6)$$

3. Results and Discussion

Figure 2 shows the changes in the density, viscosity, and conductivity properties as the molar fraction of the 2.5 M KNO_3 aqueous electrolyte is increased within the mixtures of EmimTFO. The trends illustrated that the density, viscosity, and conductivity of the electrolytes highly depend on the molar fraction of 2.5 M KNO_3 within the mixtures. A slight change in room temperature is observed due to minor variations in weather conditions during the measurement. Figures 2(a) and 2(b) illustrate that the addition of 2.5 M KNO_3 leads to a lower IL density and viscosity. This is expected due to the low density and viscosity of the aqueous solution contributing to lower values of the neat EmimTFO after dilution. In Figure 2(b), the change in viscosity is seen to be prominent when the molar fraction is 0.9, and small changes are observed from the molar fraction of 0.8 downward. This shows that a low amount of 2.5 M KNO_3 was sufficient to obtain a viscosity close to that of an aqueous electrolyte. The conductivity (Figure 2(c)) is shown to increase with the addition of 2.5 M KNO_3 which decreases the EmimTFO molar fractions in the mixture. This can be advantageous as a combination of high conductivity and low viscosity normally demonstrates high power in EDLCs [5]. Most of the ILs used for supercapacitors are reputed to have trivial conductivities [26]. The hydrophilic nature of EmimTFO enables good mixing with the 2.5 M KNO_3 and leads to better transport properties. Figure 2(d) illustrates a photograph of the single electrolyte and the prepared mixture. All the mixtures illustrated spontaneous miscibility with EmimTFO, and no biphasic states were noticed. However, little particle accumulations at the bottom of the container can be seen with $[EmimTFO]_{0.7}[2.5\text{ M } KNO_3]_{0.3}$ and $[EmimTFO]_{0.6}[2.5\text{ M } KNO_3]_{0.4}$. This phenomenon is suggested to determine the hydrophilic and miscibility limit of EmimTFO with regard to the 2.5 M KNO_3 solution.

Figure 3 illustrates the electrochemical properties of the neat EmimTFO and 2.5 M KNO_3. All electrochemical measurements were performed using MS-AC described in the experimental section as the working electrodes. Figures 3(a) and 3(b) display the CV and GCD patterns of the ionic liquid, illustrating partially-rectangular CV curves and moderately linear GCD triangles in a three-electrode measurement. These shapes represent normal pseudocapacitor behaviour, and it is noticed that EmimTFO ILs have an impact on this behaviour. EmimTFO is also responsible for the IR drop occurring in Figure 3(b) due to poor transport properties leading to non-ideal galvanostatic charge-discharge. Despite a low current response and discharge time, the electrolyte displayed an interesting potential window (0.0 to 1.1 V vs. Ag) on the positive potential and negative potential (-1.6 to 0.0 V vs. Ag). The potential window obtained on the positive and negative potentials could compare well with the previously reported three-electrode measurement utilizing hydrophobic ILs [13, 27]. Figures 3(c) and 3(d) present the results of CV and GCD patterns for the 2.5 M KNO_3 electrolyte. As displayed in Figure 3(c), the CV pattern of the 2.5 M KNO_3 electrolyte exhibits a greater current response and a more pronounced rectangular profile when compared to other electrolytes. Potassium (≈280 pm) and nitrate (≈280 μm) ion sizes are suitable for the MS-AC porous structure in enhancing the ion diffusion within the porous material's framework when using 2.5 as the molarity. This led to an ideal GCD as seen in Figure 3(d) which confirms the observations in Figure 3(c). However, the potential window on the aqueous electrolyte was limited to 0.7 and -0.9 V vs. Ag on the positive and negative potentials, respectively. The difference in equivalent series resistance (R_s) between EmimTFO and 2.5 M KNO_3 can be observed in Figure 3(e). The EmimTFO electrolyte's Nyquist plots showed a semicircular shape in the high-frequency range, showing substantial charge transfer resistance at the active material/electrolyte boundary, which supports the electrolyte's pseudocapacitive behaviour mentioned earlier. Inversely, the absence of a semicircular shape in the 2.5 M KNO_3 electrolyte highlighted the outstanding ionic conductivity and revealed a low charge transfer resistance. This is supported by the aqueous medium's short, vertically directed diffusion route.

In this section, we present an illustration of the electrochemical performance after the dilution of EmimTFO. Figure 4 illustrates the CV, GCD, and EIS results obtained with the four different mixtures: (1) $[EmimTFO]_{0.9}[2.5\text{ M } KNO_3]_{0.1}$, (2) $[EmimTFO]_{0.8}[2.5\text{ M } KNO_3]_{0.2}$, (3) $[EmimTFO]_{0.7}[2.5\text{ M } KNO_3]_{0.3}$, and (4) $[EmimTFO]_{0.6}[2.5\text{ M } KNO_3]_{0.4}$, respectively. All the electrolyte mixtures were tested within a positive potential range of 0.0 to 0.8 V vs. Ag and a negative potential range of -1.2 to 0.0 V vs. Ag. These limitations are caused by the existence of water in the mixture, which triggers oxygen and hydrogen evolutions. Many other activated carbon studies could not obtain such potential windows, especially on the negative potential, when using 2.5 M KNO_3 alone as the electrolyte [28–31]. The different potential limits are similar to the ones obtained with 2.5 M KNO_3 but with an extended potential window favoured by the presence of the EmimTFO. Figures 4(a) and 4(b) illustrate the CV curves obtained with the four distinct mixtures in the positive and negative potentials. $[EmimTFO]_{0.8}[2.5\text{ M } KNO_3]_{0.2}$ appears to have the highest current response as compared to the other mixtures. These results demonstrate the good interaction between EmimTFO and 2.5 M KNO_3 in the 0.8 to 0.2 molar fraction which triggered a high migration of ions across the carbon material interface. Additionally, this mixture allowed a significant amount of inaccessible micropores to be polarized because of the decent electrode surface wettability occurring when it is used as an electrolyte, thus yielding high ionic conductivity and great electrochemical performances. A clear decline in the current response is observed for $[EmimTFO]_{0.7}[2.5\text{ M } KNO_3]_{0.3}$ and $[EmimTFO]_{0.6}[2.5\text{ M } KNO_3]_{0.4}$. Figures 4(c)

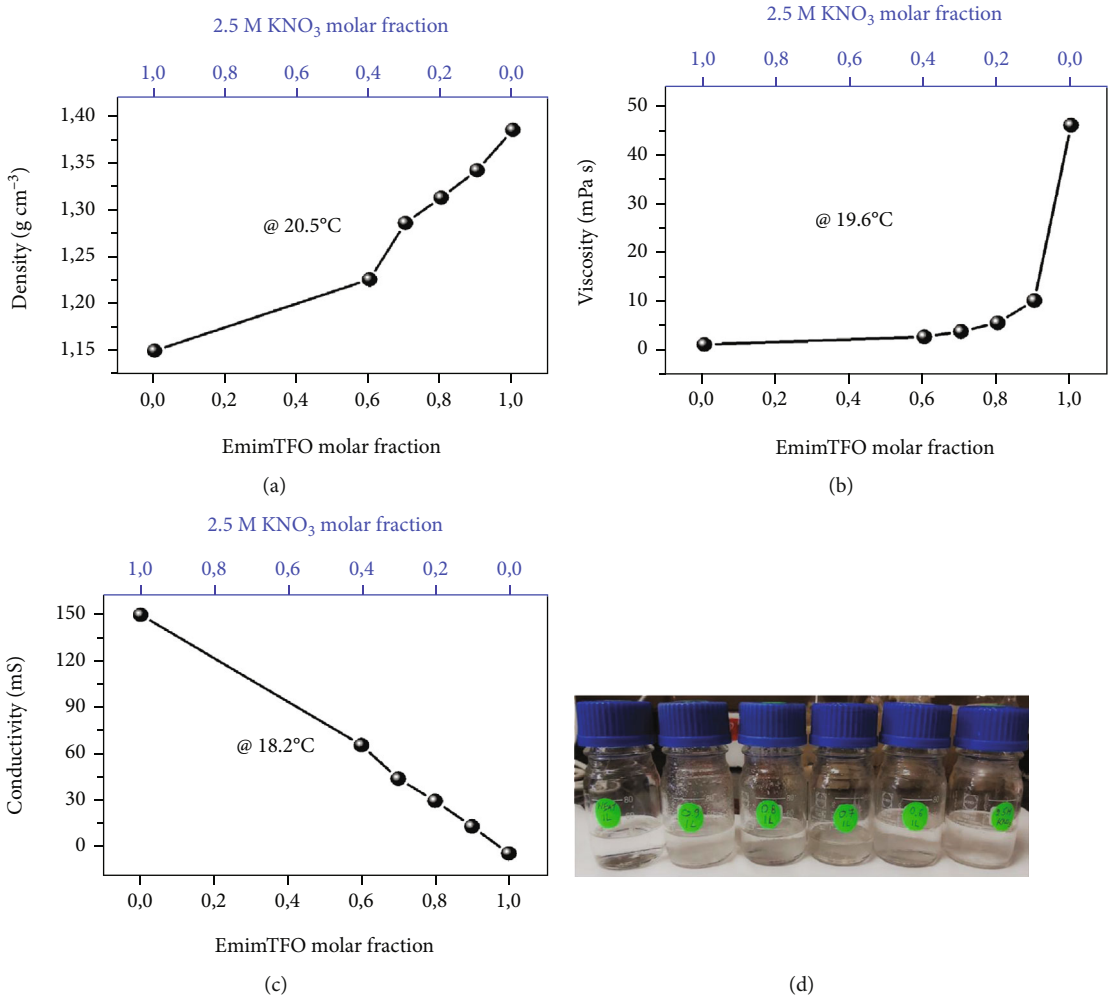

Figure 2: (a) Density, (b) viscosity, and (c) conductivity measurements of EmimTFO, 2,5 M KNO_3, and (d) EmimTFO mixtures diluted with 2.5 M KNO_3 by molar fractions of 0.6, 0.7, 0.8, and 0.9, respectively.

and 4(d) illustrate the distinct four mixtures' GCD curves on both potentials. In this case, $[EmimTFO]_{0.8}[2.5\,M\ KNO_3]_{0.2}$ also demonstrated longer discharge times on both the positive and negative potentials, confirming the high current response demonstrated in the CV curves. This is due to the improved transport properties acquired by combining the two electrolyte mediums, resulting in a larger charge build-up on the electrodes. The IR drop observed in Figure 3(c) with the $[EmimTFO]_{0.9}[2.5\,M\ KNO_3]_{0.1}$ electrolyte is less significant for the $[EmimTFO]_{0.8}[2.5\,M\ KNO_3]_{0.2}$ and the other electrolytes, as displayed in Figure 4(c). This confirms the ideal interaction at the electrode/electrolyte interface when using $[EmimTFO]_{0.8}[2.5\,M\ KNO_3]_{0.2}$.

Figures 5(a) and 5(b) illustrate a plot of several specific capacities since the materials show semilinear GCD curves against different specific currents determined for the four electrolyte mixtures in the positive and negative potentials calculated using Equation (2). The mixture $[EmimTFO]_{0.8}[2.5\,M\ KNO3]_{0.2}$ demonstrates high specific capacity on both potentials. The electrolyte generated specific capacities of 40.2 and 85.8 mAh g^{-1} on the positive and negative potentials, respectively, at 0.25 A g^{-1}. $[EmimTFO]_{0.8}[2.5\,M\ KNO_3]_{0.2}$ also exhibited a sustaining capacity retention equivalent to 40% and 48% of its original capacity when raising the specific current to 2 A g^{-1} on the negative and positive potentials, respectively. Figure 5(d) illustrates the EIS measurement obtained with the four mixtures. The figure displays a distinct semicircle in the region of high frequency for all the mixtures. However, $[EmimTFO]_{0.8}[2.5\,M\ KNO3]_{0.2}$ displays a less pronounced semicircle indicating minimal charge transfer resistance at the electrolyte/electrode interface [32, 33]. The mixtures demonstrated R_s values of 3.8, 2.5, 5.5, and 3.3 Ω for $[EmimTFO]_{0.9}[2.5\,M\ KNO3]_{0.1}$, $[EmimTFO]_{0.8}[2.5\,M\ KNO3]_{0.2}$, $[EmimTFO]_{0.7}[2.5\,M\ KNO3]_{0.3}$, and $[EmimTFO]_{0.6}[2.5\,M\ KNO3]_{0.4}$, respectively. The low R_s value obtained with $[EmimTFO]_{0.8}[2.5\,M\ KNO3]_{0.2}$ illustrates its enhanced conductivity and faster mass transport on the electrode's interface as compared to the other mixtures. $[EmimTFO]_{0.8}[2.5\,M\ KNO3]_{0.2}$ is therefore considered to be an optimal mixture to achieve good ion diffusion and adsorptions in this study.

Figure 6 illustrates a comparison of the electrochemical properties of MS-AC//MS-AC symmetric devices assembled

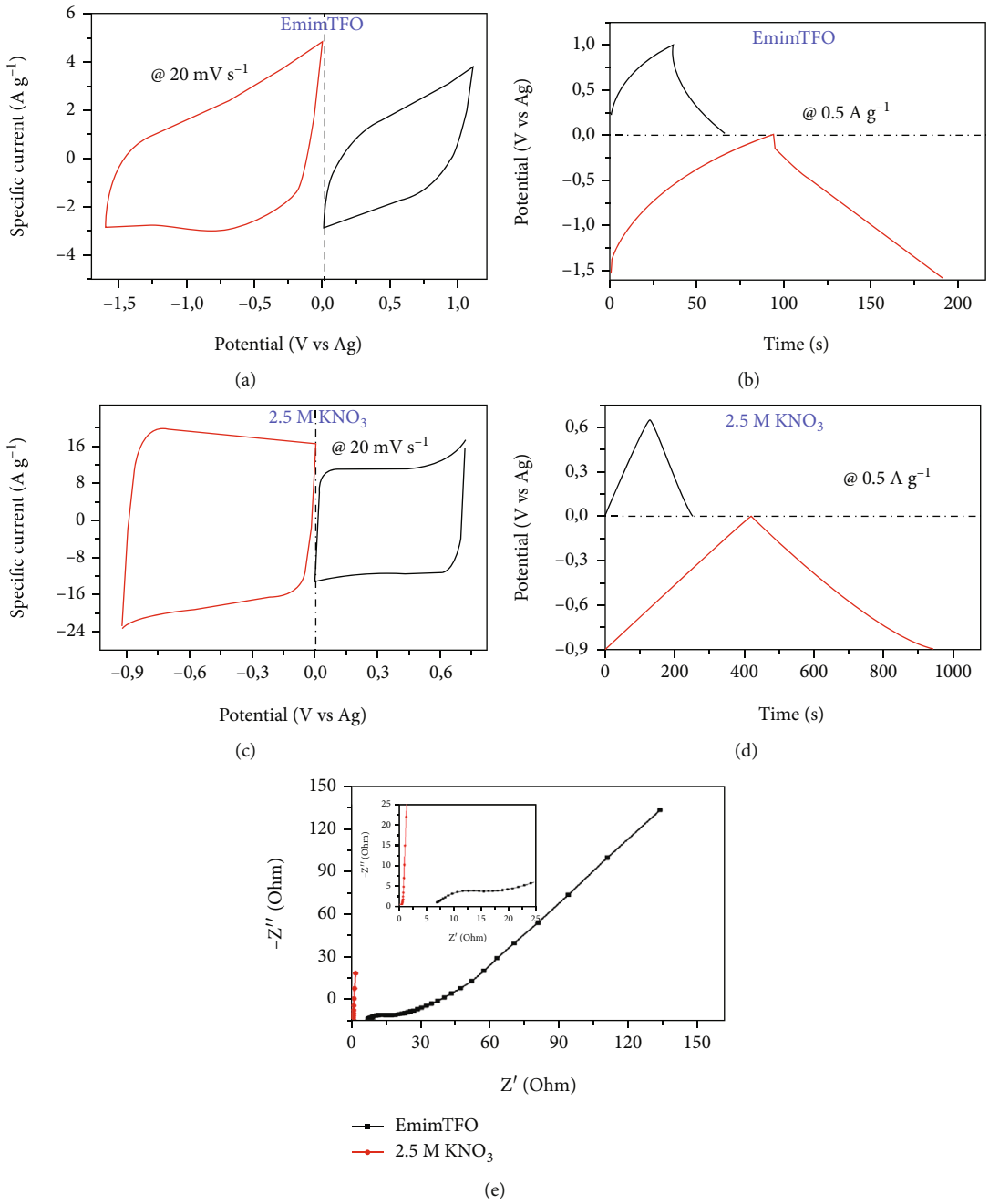

Figure 3: (a, c) Positive and negative curves for electrode CV analysis at 20 mV s^{-1}, (b, d) positive and negative curves of electrode GCD analysis at 0.5 A g^{-1}, and (e) EIS Nyquist plot for neat EmimTFO and 2.5 M KNO_3, respectively (the inset indicates the low-frequency region).

with EmimTFO, 2.5 M KNO_3, and the mixture $[EmimTFO]_{0.8}[2.5\,M\ KNO_3]_{0.2}$ as electrolytes. The mixture $[EmimTFO]_{0.8}[2.5\,M\ KNO_3]_{0.2}$ was selected for the full device because it showed superior electrochemical results as compared to other mixtures. The CV curves of the devices assembled with different electrolytes at a scan rate of 20 mV s^{-1} are displayed in Figure 6(a). The 2.5 M KNO_3 demonstrated the highest current response at a cell voltage of 1.6 V. This electrolyte shows a voltage window limitation as it is a water-based electrolyte. The EmimTFO device displayed the advantage of a water-free electrolyte which reached 2.6 V. Yet, its low conductivity led to a low current response as compared to the other two electrolytes. The $[EmimTFO]_{0.8}[2.5\,M\ KNO_3]_{0.2}$ device illustrated EDLC behaviour up to a voltage window of 2.1 V while displaying a higher current response compared to the EmimTFO device. This result of the $[EmimTFO]_{0.8}[2.5\,M\ KNO_3]_{0.2}$ electrolyte mixture is promising as it enabled voltage extension compared to KNO_3 electrolyte with a better current response as compared to EminTFO electrolyte which indicates the improvement in ionic conductivity within the device. Furthermore, the voltage extension will also be

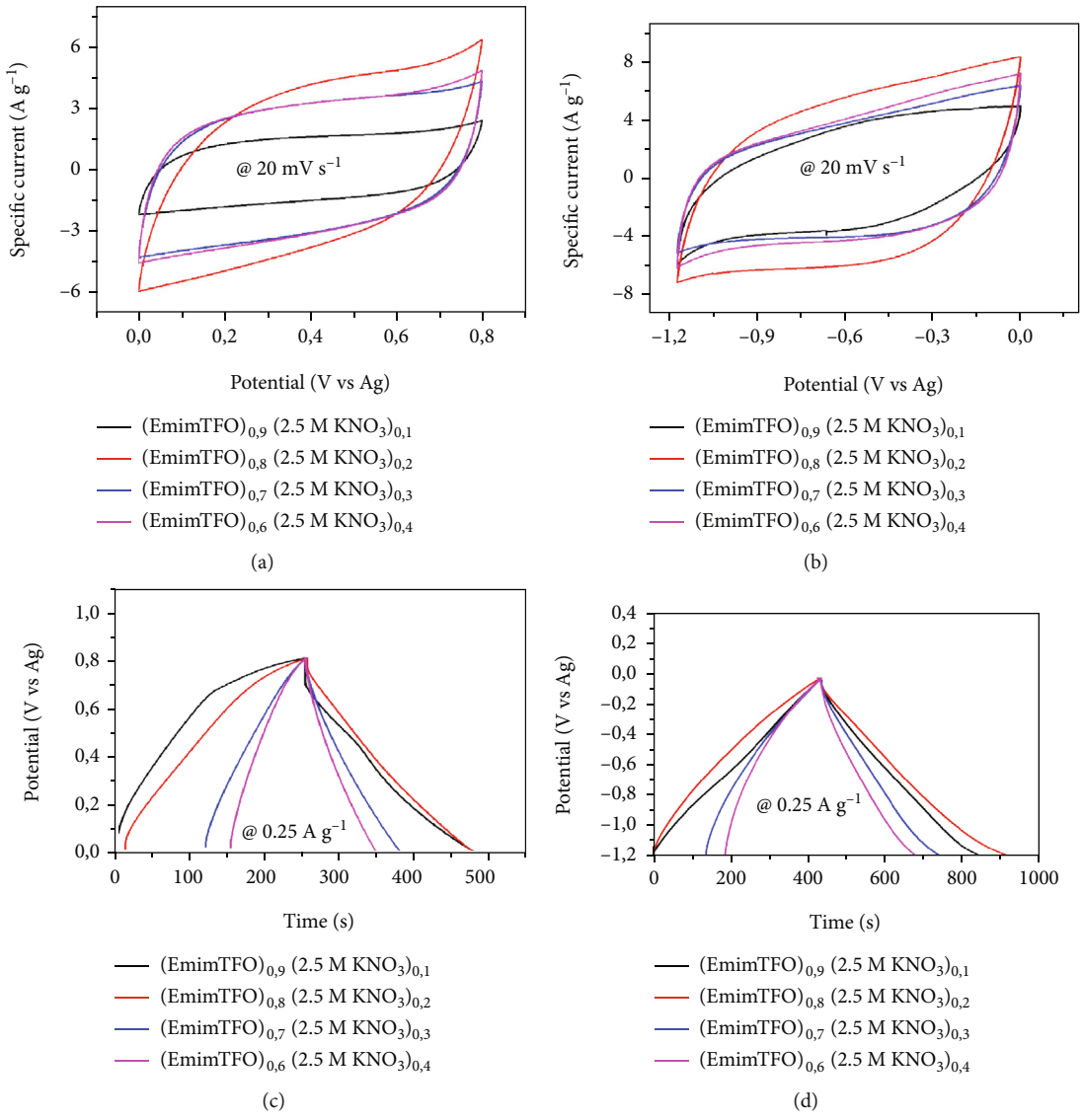

Figure 4: (a, b) CV patterns at 20 mV s^{-1} in both positive and negative potentials, (c, d) GCD patterns at 0.5 A g^{-1} in both positive and negative potentials, comparing the use of EmimTFO mixtures diluted with 2.5 M KNO_3 by molar fractions of 0.6, 0.7, 0.8, and 0.9.

beneficial for enhancing the specific energy (E_s). Figure 6(b) shows the linear EDLC behaviour for the GCD patterns of the devices in these three different electrolytes. A higher charge-discharge time for the $[EmimTFO]_{0.8}[2.5\,M\ KNO_3]_{0.2}$ MS-AC//MS-AC device is observed. This is due to the improved viscosity and conductivity which contributed toward having a higher number of ions diffusing within the porous material. The EIS Nyquist plot for the three devices is displayed in Figure 6(c). The addition of 2.5 M KNO_3 to the $[EmimTFO]_{0.8}[2.5\,M\ KNO_3]_{0.2}$ mixture lowers the semicircle that is observed when the EmimTFO electrolyte is used alone. Also, the device displayed a short diffusion length, with its slope being closer to the vertical axis mirroring the ideal supercapacitor. Despite its R_s value of 2.68 Ω, the overall EIS results show that the $[EmimTFO]_{0.8}[2.5\,M\ KNO_3]_{0.2}$ electrolyte yielded a low charge transfer resistance, promoted by the good ionic conductivity within the device.

Figure 7 provides the full electrochemical results of the $[EmimTFO]_{0.8}[2.5\,M\ KNO_3]_{0.2}$ MS-AC//MS-AC symmetric device. The device's CV curves at multiple scan rates are shown in Figure 7(a). Typical EDLC behaviour can be noticed from the curves having almost rectangular shapes. The GCD triangles are displayed in Figure 7(b). The figure illustrated a reversible path which confirms the EDLC behaviour. A slight bend is observed at approximately 2.1 V with the curve running at 0.5 A g^{-1}. This was used as an indication to determine the maximum voltage at which the device could operate as the undulation may indicate electrolyte deterioration taking place in the device. The CVs and GCDs obtained in Figures 7(a) and 7(b) further confirm the EDLC behaviour in the assembled device. The specific capacitance of the single electrode in the device is illustrated in Figure 7(c) and calculated using an equation (3). At a current density of 0.5 A g^{-1}, it exhibits a specific capacitance of

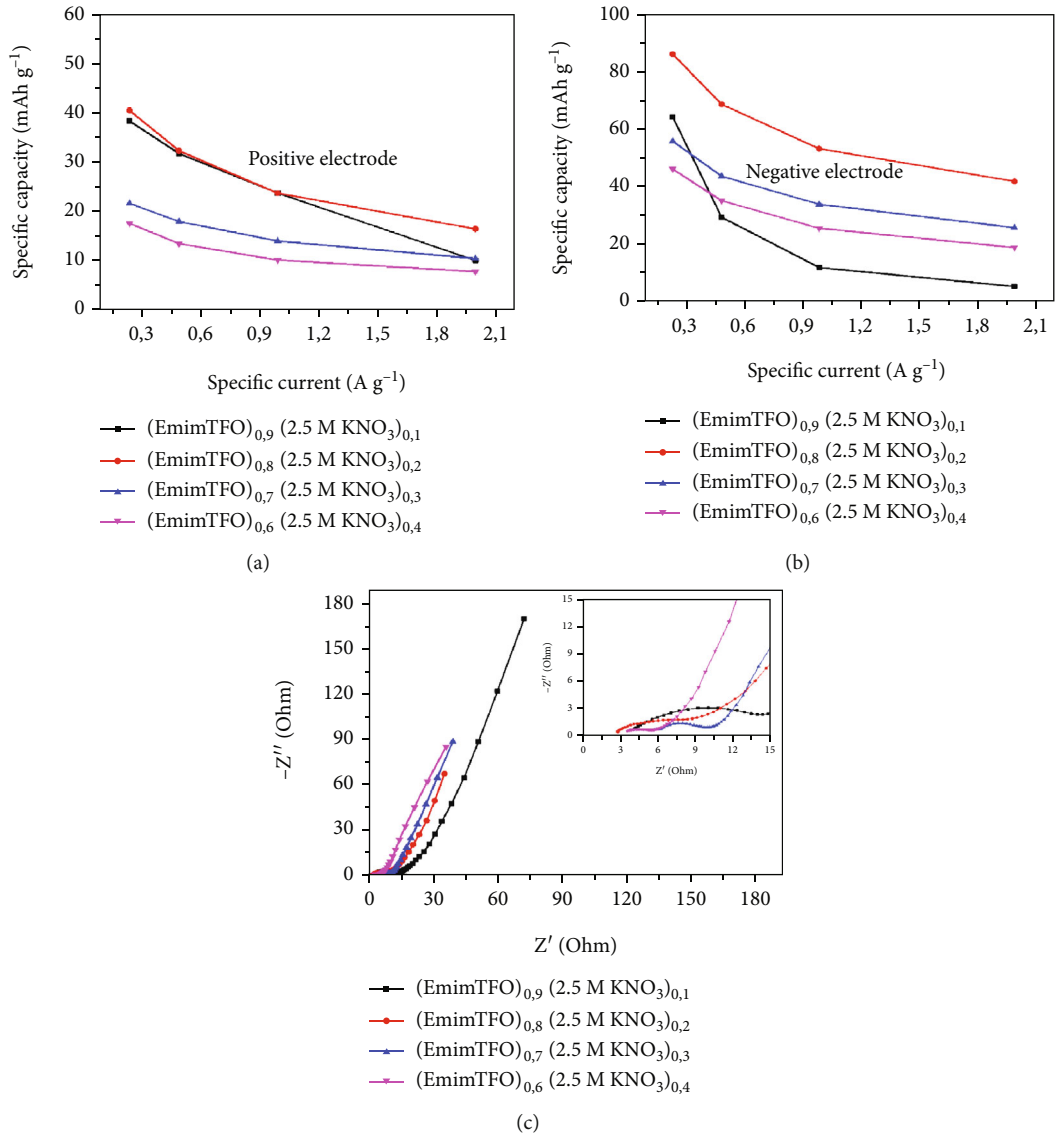

FIGURE 5: Positive (a) and negative (b) electrode specific capacities against the specific current and (c) an EIS Nyquist plot comparing the use of EmimTFO mixtures diluted with 2.5 M KNO_3 by molar fractions of 0.6, 0.7, 0.8, and 0.9 (inset figure showing the low-frequency region).

138.62 F g^{-1}. Even when the current density reached 5 A g^{-1}, the device could still maintain 40% of its original value with a specific capacitance of 55.08 F g^{-1}. The Nyquist plot as well as the equivalent circuit (inset to the figure) for the [EmimTFO]$_{0.8}$[2.5 M KNO$_3$]$_{0.2}$ devices is presented in Figure 7(d). The fitting was accomplished using a complex nonlinear least square program using the equivalent circuit. The device's Nyquist plot demonstrates a low semicircle that is brought due to small charge transfer resistance (R_{CT}) at the electrode and electrolyte interface. The obtained R_s and R_{CT} values were 2.7 Ω and 3.4 Ω, respectively, for the experimental/fitting curve. The slow adsorption process, which occurs because of the complex mixture of ions, is suggested to be the root cause of this resistance. [34]. The R_s element in the circuit is linked to the conductivity of the electrolyte mixture toward the electrode materials. Furthermore, the Warburg element (Z_w) which is also present in the circuit represents the mass-transport process of ions that takes place at the electrode/electrolyte interface [35]. This process is also associated with the mass capacitance, Q, in the circuit. The C element in the circuit indicates that the device behaves like a capacitor. The symmetric device bode plot is illustrated in Figure 7(e). The figure indicates a device's phase angle of -70.1° which is close to the ideal capacitor phase angle of -90°. The inset to Figure 7(e) illustrates a photograph whereby the [EmimTFO]$_{0.8}$[2.5 M KNO$_3$]$_{0.2}$ device powered 4 light-emitting diodes (LED) connected in parallel which requires at least 1.8 V. This illustrates the extent to which the assembled device can be applied. Figure 7(f) presents the real (C') and imaginary (C'') capacitance values of the [EmimTFO]$_{0.8}$[2.5 M KNO$_3$]$_{0.2}$ device as a function of frequency. It was observed that the imaginary capacitance value, C'', reaches its peak value at a frequency of approximately 0.02 Hz, which corresponds to a relaxation time of

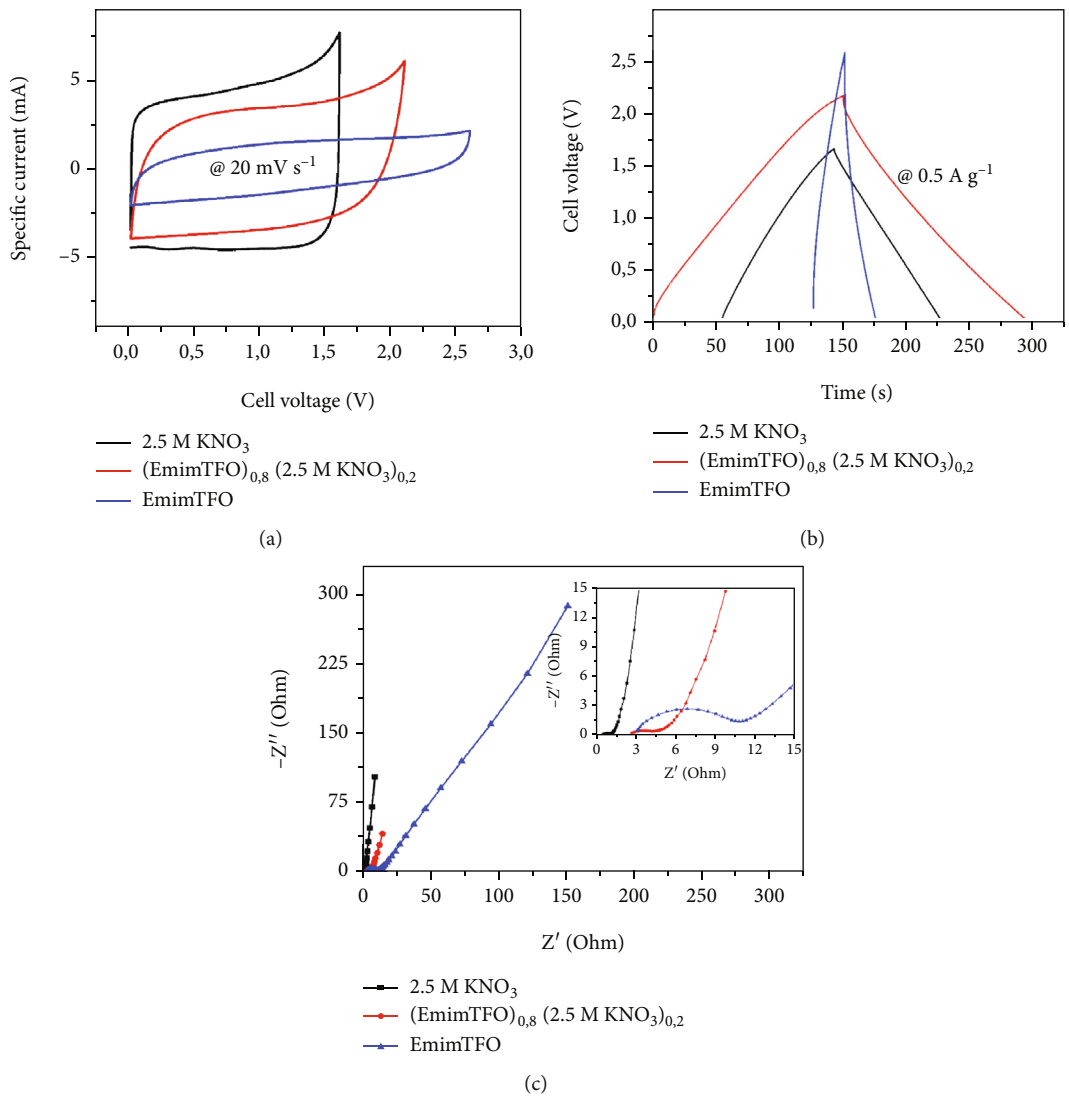

Figure 6: (a) CV curves at 20 mV s^{-1}, (b) GCD curves at 0.5 A g^{-1}, (c) EIS Nyquist plot comparing the device assembled using 2.5 M KNO_3, EmimTFO, and 0.8 molar fraction diluted EmimTFO mixture.

3.54 seconds. This relaxation time is the minimum duration for the device to be completely charged. These results suggest that this device can attain full charge in a notably short time.

Figure 8(a) illustrates the Coulombic efficiency of all the devices with an overall performance above 99% up to 10,000 cycles. Figure 8(b) displays the retention in capacitance of the devices after 10,000 charge-discharge cycles with percentages of 94.7, 71.4, and 88.5 for the 2.5 M KNO_3, the $[EmimTFO]_{0.8}[2.5\,M\ KNO_3]_{0.2}$, and EmimTFO electrolytes-based devices, respectively. The minor decline in capacitance retention occurring with the $[EmimTFO]_{0.8}[2.5\,M\ KNO_3]_{0.2}$ device after performing 6000 charge-discharge cycles may be related to the water content within the mixture which disturbed the device's electrochemical stability. Figure 8(c) presents the Ragone plot that shows the correlation between the specific power and specific energy of the device. The plot demonstrates the essence of this investigation as the $[EmimTFO]_{0.8}[2.5\,M\ KNO_3]_{0.2}$ is seen to increase the range of the specific energy. The specific energies (E_s) for the $[EmimTFO]_{0.8}[2.5\,M\ KNO_3]_{0.2}$ device obtained at various specific currents varied between 22.2 Wh kg^{-1} and 8.4 Wh kg^{-1} with specific powers (Ps) varying between 153.8 W·kg^{-1} and 1458.3 Wkg^{-1}. The specific energies of the $[EmimTFO]_{0.8}[2.5\,M\ KNO_3]_{0.2}$ device surpassed those obtained with the other two assembled devices which illustrated maximum E_s values of 11.2 Wh kg^{-1} for 2 M KNO_3 and 4.7 Wh kg^{-1} for EmiTFO when evaluated in the same specific currents. These results demonstrate the highly efficient reversible adsorption and desorption of electrolyte ions which can be achieved through the dilution of compatible ionic liquid electrolytes. A comparison of the performance of dual-electrolytes (ionic liquid-aqueous electrolytes) in symmetric configurations is shown in Table 2. The $[EmimTFO]_{0.8}[2.5\,M\ KNO_3]_{0.2}$ electrolyte can be seen to outperform or match the previously reported devices based on numerous parameters. The outstanding specific energy obtained could be directly related to the wider cell voltage and improved transport properties obtained from merely mixing 2.5 M KNO_3 and EmimTFO in an optimised ratio. This electrolyte

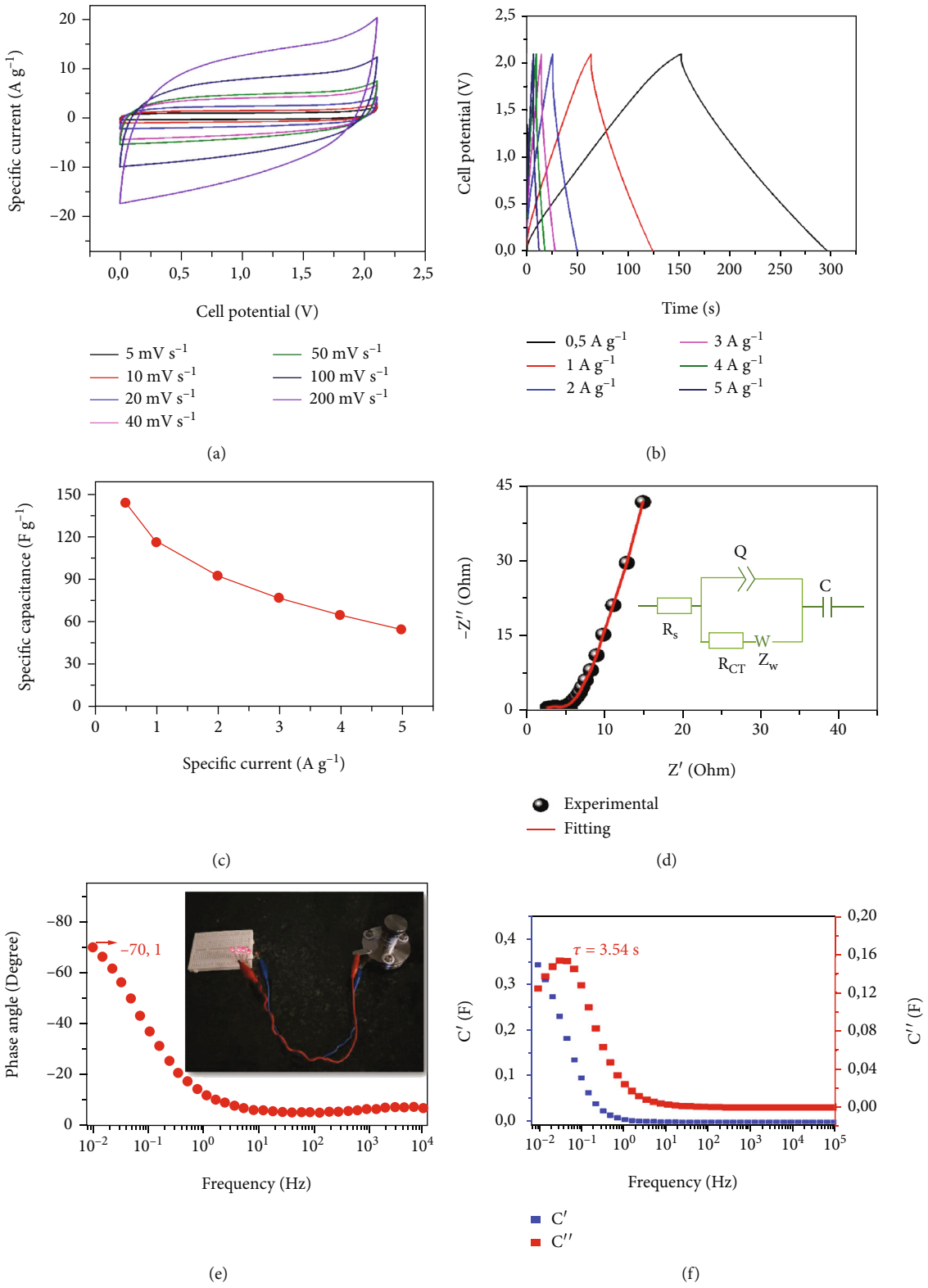

FIGURE 7: (a) CV curves measured at different scan rates, (b) GCD curves measured at various specific currents, (c) specific capacitance and specific current relationship, (d) fitting of EIS Nyquist plot (inset equivalent series circuit), (e) phase angle as a function of frequency (with a photograph of the device powering LEDs (light-emitting diodes) in the inset). (f) Real and imaginary plots of the capacitance vs. frequency for the device assembled with $[EmimTFO]_{0.8}[2.5\,M\ KNO_3]_{0.2}$ as the electrolyte.

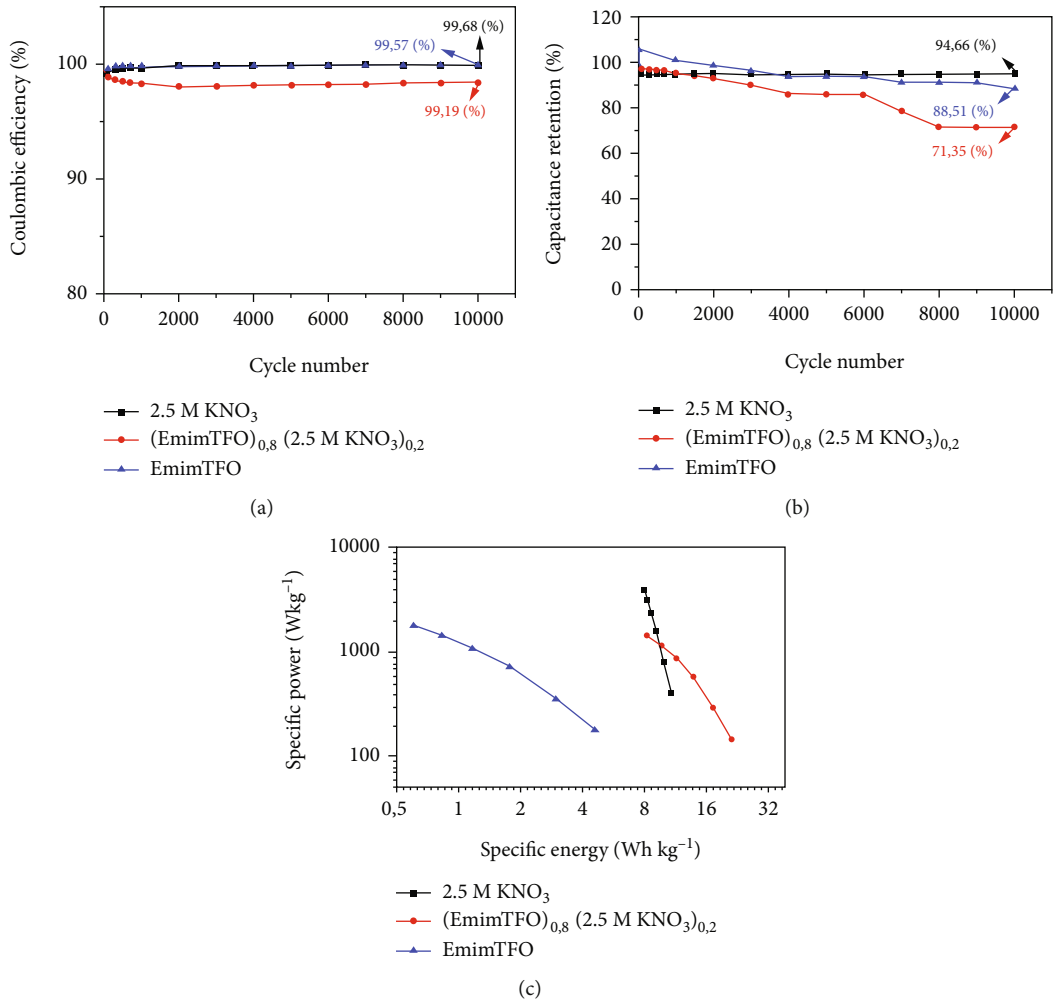

FIGURE 8: (a) Coulombic efficiency against a number of cycles, (b) capacitance retention against a number of cycles, and (c) Ragone plot comparing the device assembled using 2.5 M KNO_3, EmimTFO, and 0.8 molar fraction diluted EmimTFO mixture.

TABLE 2: Ionic liquid-aqueous electrolyte symmetric devices performances comparison.

Material	Electrolyte	C_{single} ($F\,g^{-1}$)	Cell voltage (V)	E_S ($Wh\,kg^{-1}$)	Ps ($W\,Kg^{-1}$)	Ref.
CNT/AC	1 M $H_2SO_{4(aq)}$/$EAN_{(IL)}$ (ion-exchange membrane separation)	10.0	1.60	N/A	N/A	[36]
AC/AC	1 M LiTFSI $_{(aq.)}$/$MPPyrroTFSI_{(IL)}$	131	2.20	22.6	N/A	[23]
AC/AC	[Pyrr][$MeSO_3$]+H_2O	97	0.80	4.00	1390	[14]
MWCNT/MWCNT	EMImFAP to PVdF-HFP (4 to 1)	26.6	2.6	17.2	1890	[37]
AC/AC	Al/C/SPSU/%3$nSiO_2$/0.2IL/C/Al	134	1	18.6	1089	[38]
AC/AC	SPSU/%5 hBN/0.2 IL	90.4	1	43.8	1100	[39]
AC/AC	$[EmimTFO]_{0.8}[2.5\ M\ KNO_3]_{0.2}$	138.6	2.10	24.5	4000	This work

mixture could be easily reproduced and used with other capacitive materials to boost the specific energy which is a critical factor in supercapacitor applications.

4. Conclusion

A successful investigation of the dilution effect on EmimTFO using 2.5 M KNO_3 toward higher electrochemical performances was conducted. The transport properties of EmimTFO as well as mixtures diluted with 2.5 M KNO_3 by molar fractions of 0.6, 0.7, 0.8, and 0.9 were investigated. Despite a minor decline in potential windows from -1.6 to -1.2 V vs. Ag on the negative potential and 0.8 to 1.0 V vs. Ag on the positive potential due to the presence of water, the addition of the 2.5 M KNO_3 solution generated higher specific capacities C_{sp} (~40.2 mAh g^{-1} for $C_{Sp}{}^{+}$ and ~85.8 mAh g^{-1} for

C_{Sp}^{-}) than the neat EmimTFO in a three-electrode measurement ran at 0.25 A g^{-1}, whereby activated carbon was used as the electrode material. These potential windows are wider than the ones previously obtained when using 2.5 M KNO_3 electrolyte. $[EmimTFO]_{0.8}[2.5\ M\ KNO_3]_{0.2}$ was then used to build an MS-AC//MS-AC supercapacitor that could run at an operating voltage of 2.1 V. The device exhibited stable charge-discharge cycling over 10,000 cycles, with a capacitance retention of 71.35%. Additionally, the device demonstrated a high specific energy of 22.21 Wh kg^{-1} and a specific power of 520 W kg^{-1} at a current density of 0.5 A g^{-1}. This electrolyte mixing technique proved its advantages in enhancing the specific energy of the supercapacitor which is a critical factor for this application.

Data Availability

Data is available on request from Prof. Ncholu Manyala at email: ncholu.manyala@up.ac.za.

Conflicts of Interest

The authors declare that there is no conflict of interest.

Acknowledgments

The authors wish to extend their appreciation to the Department of Science and Technology (DST) and the National Research Foundation of South Africa (NRF) with grant no. 61056 for their generous financial support that enabled the completion of this research, Open Access funding enabled and organized by SANLiC Gold. The observations, findings, and conclusions outlined in this report are solely those of the authors, and the NRF does not assume any responsibility or liability in this regard. Vianney N. Kitenge would also like to acknowledge the financial support received from the University of Pretoria for his Ph.D. studies.

References

[1] J. Yan, Q. Wang, T. Wei, and Z. Fan, "Recent advances in design and fabrication of electrochemical supercapacitors with high energy densities," *Advanced Energy Materials*, vol. 4, no. 4, article 1300816, 2014.

[2] G. Wang, L. Zhang, and J. Zhang, "A review of electrode materials for electrochemical supercapacitors," *Chemical Society Reviews*, vol. 41, no. 2, pp. 797–828, 2012.

[3] P. Simon and Y. Gogotsi, "Perspectives for electrochemical capacitors and related devices," *Nature Materials*, vol. 19, no. 11, pp. 1151–1163, 2020.

[4] P. Simon and Y. Gogotsi, *Materials for Electrochemical Capacitors*, Co-Published with Macmillan Publishers Ltd, UK, 2009.

[5] F. Béguin, V. Presser, A. Balducci, and E. Frackowiak, "Carbons and electrolytes for advanced supercapacitors," *Advanced Materials*, vol. 26, no. 14, pp. 2219–2251, 2014.

[6] C. Zhong, Y. Deng, W. Hu, J. Qiao, L. Zhang, and J. Zhang, "A review of electrolyte materials and compositions for electrochemical supercapacitors," *Chemical Society Reviews*, vol. 44, no. 21, pp. 7484–7539, 2015.

[7] S. Zhang and N. Pan, "Supercapacitors performance evaluation," *Advanced Energy Materials*, vol. 5, no. 6, article 1401401, 2015.

[8] P. M. Yeletsky, M. V. Lebedeva, and V. A. Yakovlev, "Today's progress in the synthesis of porous carbons from biomass and their application for organic electrolyte and ionic liquid based supercapacitors," *Journal of Energy Storage*, vol. 50, article 104225, 2022.

[9] E. Frackowiak and F. Béguin, "Carbon materials for the electrochemical storage of energy in capacitors," *Carbon*, vol. 39, no. 6, pp. 937–950, 2001.

[10] B. Pal, S. Yang, S. Ramesh, V. Thangadurai, and R. Jose, "Electrolyte selection for supercapacitive devices: a critical review," *Nanoscale Advances*, vol. 1, no. 10, pp. 3807–3835, 2019.

[11] M. Armand, F. Endres, D. R. MacFarlane, H. Ohno, and B. Scrosati, "Ionic-liquid materials for the electrochemical challenges of the future," *Nature Materials*, vol. 8, no. 8, pp. 621–629, 2009.

[12] N. Yaghini, L. Nordstierna, and A. Martinelli, "Effect of water on the transport properties of protic and aprotic imidazolium ionic liquids – an analysis of self-diffusivity, conductivity, and proton exchange mechanism," *Physical Chemistry Chemical Physics*, vol. 16, no. 20, pp. 9266–9275, 2014.

[13] D. Momodu, N. F. Sylla, B. Mutuma et al., "Stable ionic-liquid-based symmetric supercapacitors from capsicum seed-porous carbons," *Journal of Electroanalytical Chemistry*, vol. 838, pp. 119–128, 2019.

[14] M. Anouti, E. Couadou, L. Timperman, and H. Galiano, "Protic ionic liquid as electrolyte for high-densities electrochemical double layer capacitors with activated carbon electrode material," *Electrochimica Acta*, vol. 64, pp. 110–117, 2012.

[15] S. Zhang, J. Zhang, Y. Zhang, and Y. Deng, "Nanoconfined ionic liquids," *Chemical Reviews*, vol. 117, no. 10, pp. 6755–6833, 2017.

[16] A. Brandt, S. Pohlmann, A. Varzi, A. Balducci, and S. Passerini, "Ionic liquids in supercapacitors," *MRS Bulletin*, vol. 38, no. 7, pp. 554–559, 2013.

[17] A. Balducci, F. Soavi, and M. Mastragostino, "The use of ionic liquids as solvent-free green electrolytes for hybrid supercapacitors," *Applied Physics A*, vol. 82, no. 4, pp. 627–632, 2006.

[18] E. P. Yambou and B. G. F. Béguin, "Binary mixtures of ionic liquids based on EMIm cation and fluorinated anions: physico-chemical characterization in view of their application as low- temperature electrolytes," *Journal of Molecular Liquids*, vol. 298, article 111959, 2020.

[19] L. Timperman, A. Vigeant, and M. Anouti, "Eutectic mixture of protic ionic liquids as an electrolyte for activated carbon-based supercapacitors," *Electrochimica Acta*, vol. 155, pp. 164–173, 2015.

[20] E. Rilo, J. Vila, A. M. Garcí, L. M. Varela, and O. Cabeza, "Viscosity and electrical conductivity of binary mixtures of CnMIM-BF4with ethanol at 288 K, 298 K, 308 K, and 318 K," *Journal of Chemical & Engineering Data*, vol. 55, no. 11, pp. 5156–5163, 2010.

[21] R. Palm, H. Kurig, K. Tõnurist, A. Jänes, and E. Lust, "Electrical double layer capacitors based on 1-ethyl-3-methylimidazolium tetrafluoroborate with small addition of acetonitrile," *Electrochimica Acta.*, vol. 85, pp. 139–144, 2012.

[22] V. V. Chaban, I. V. Voroshylova, O. N. Kalugin, and O. V. Prezhdo, "Acetonitrile boosts conductivity of imidazolium ionic liquids," *The Journal of Physical Chemistry B*, vol. 116, no. 26, pp. 7719–7727, 2012.

[23] S. Sethuraman and S. Montree, "A simple and practical hybrid ionic liquid/aqueous dual electrolyte configuration for safe and ion-exchange membrane-free high cell potential supercapacitor," *Electrochimica Acta*, vol. 305, pp. 443–451, 2019.

[24] M. Anouti, M. Caillon-Caravanier, Y. Dridi, H. Galiano, and D. Lemordant, "Synthesis and characterization of new pyrrolidinium based protic ionic liquids. Good and superionic liquids," *The Journal of Physical Chemistry B*, vol. 112, no. 42, pp. 13335–13343, 2008.

[25] V. Kitenge, D. Tarimo, K. Oyedotun, G. Rutavi, and N. Manyala, "Facile and sustainable technique to produce low-cost high surface area mangosteen shell activated carbon for supercapacitors applications," *Journal of Energy Storage*, vol. 56, article 105876, 2022.

[26] A. Balducci, S. S. Jeong, G. T. Kim et al., "Development of safe, green and high performance ionic liquids-based batteries (ILLIBATT project)," *Journal of Power Sources*, vol. 196, no. 22, pp. 9719–9730, 2011.

[27] A. Eftekhari, "Supercapacitors utilising ionic liquids," *Energy Storage Materials*, vol. 9, pp. 47–69, 2017.

[28] D. T. Bakhoum, K. O. Oyedotun, S. Sarr et al., "A study of porous carbon structures derived from composite of cross-linked polymers and reduced graphene oxide for supercapacitor applications," *Journal of Energy Storage*, vol. 51, article 104476, 2022.

[29] B. K. Mutuma, N. F. Sylla, A. Bubu et al., "Valorization of biodigestor plant waste in electrodes for supercapacitors and microbial fuel cells," *Electrochimica Acta*, vol. 391, article 138960, 2021.

[30] N. F. Sylla, N. M. Ndiaye, B. D. Ngom et al., "Effect of porosity enhancing agents on the electrochemical performance of high-energy ultracapacitor electrodes derived from peanut shell waste," *Scientific Reports*, vol. 9, no. 1, p. 9, 2019.

[31] D. J. Tarimo, K. O. Oyedotun, A. A. Mirghni, N. F. Sylla, and N. Manyala, "High energy and excellent stability asymmetric supercapacitor derived from sulphur-reduced graphene oxide/manganese dioxide composite and activated carbon from peanut shell," *Electrochimica Acta*, vol. 353, article 136498, 2020.

[32] V. N. Kitenge, K. O. Oyedotun, O. Fasakin et al., "Enhancing the electrochemical properties of a nickel–cobalt-manganese ternary hydroxide electrode using graphene foam for supercapacitors applications," *Materials for Renewable and Sustainable Energy*, vol. 10, no. 1, 2021.

[33] D. J. Tarimo, A. A. Mirghni, K. O. Oyedotun, G. Rutavi, V. N. Kitenge, and N. Manyala, "Recycling of biomass wastes from amarula husk by a modified facile economical water salt method for high energy density ultracapacitor application," *Journal of Energy Storage*, vol. 53, article 105166, 2022.

[34] M. Eikerling, A. A. Kornyshev, and E. Lust, "Optimized structure of nanoporous carbon-based double-layer capacitors," *Journal of The Electrochemical Society*, vol. 152, no. 1, p. E24, 2005.

[35] K. TõNurist, A. JäNes, T. Thomberg, H. Kurig, and E. Lust, "Influence of mesoporous separator properties on the parameters of electrical double-layer capacitor single cells," *Journal of The Electrochemical Society*, vol. 156, no. 4, p. A334, 2009.

[36] P. F. R. Ortega, Z. González, C. Blanco, G. G. Silva, R. L. Lavall, and R. Santamaría, "Biliquid supercapacitors: a simple and new strategy to enhance energy density in asymmetric/hybrid devices," *Electrochimica Acta*, vol. 254, pp. 384–392, 2017.

[37] G. P. Pandey and S. A. Hashmi, "Performance of solid-state supercapacitors with ionic liquid 1-ethyl-3-methylimidazolium tris(pentafluoroethyl) trifluorophosphate based gel polymer electrolyte and modified MWCNT electrodes," *Electrochimica Acta*, vol. 105, pp. 333–341, 2013.

[38] S. T. Gunday, E. Cevik, A. Yusuf, and A. Bozkurt, "Synthesis, characterization and supercapacitor application of ionic liquid incorporated nanocomposites based on SPSU/silicon dioxide," *Journal of Physics and Chemistry of Solids*, vol. 137, article 109209, 2020.

[39] S. T. Gunday, E. Cevik, A. Yusuf, and A. Bozkurt, "Nanocomposites composed of sulfonated polysulfone/hexagonal boron nitride/ionic liquid for supercapacitor applications," *Journal of Energy Storage*, vol. 21, pp. 672–679, 2019.